Sudan University of Science and Technology
College of Graduate Studies

# Investigation of Structural and Optical Properties of Zinc Chromate Nanocrystals Prepared by Hydrothermal and Combustion Methods

# تقصي التركيب و الخصائص البصرية لبلورات كرومات الزنك النانوية المحضرة بالطريقة الحرارية المائية و طريقة الإحتراق

**A Dissertation Submitted in Partial Fulfilment for the Requirement of a Master Degree (M.Sc) in Physics**

**Prepared by**
**Marwa Hamadalniel Mohamed Suliman**

**Supervised by**
**Dr. Nadir S.E. Osman**

**July 2019**

# الآية

بسم الله الرحمن الرحيم

{أَمَّنْ هُوَ قانتٌ آناءَ اللَّيلِ سَاجِداً وَقَائِماً يَحذَرُ الآخِرةَ ويَرجُو رَحَمةَ ربِّهِ قُلْ هل يَسْتَوى الَّذينَ يَعْلَمُونَ والَّذينَ لَايَعْلَمُونَ إِنَّما يَتَذكَّرُ أُوْلُوا الأَلْبابِ}

الزمر آية (9).

# Acknowledgments

First and foremost, I would like to express my sincere gratitude to my supervisor Dr. Nadir S.E. Osman for his guidance and encouragement during this work. His knowledge and experience have been a path of illumination for me to finish this work. I am indebted to him for the boundless support, valuable comments, and professional advice which make this dissertation a reality.

Great acknowledge to my brother Munzir H. Mohamed at King Fahad University for Minerals and Petroleum for his support and help in this work.

I also would like to acknowledge Africa City of Technology for providing equipment that was used to synthesize the materials for this work.

Furthermore, many thanks are due to staff members of the Department of Physics at Sudan University of Science and Technology for being as a family.

My heartfelt gratitude to all of my teachers upon the long journey of education. During this journey, I was extraordinarily fortunate in having many nice teachers who gave interesting feedback and valuable lessons in different knowledge, as well as overcome many hard times. Without them, I would never be able to love and carry out my studies. I am sorry that no names are written, but indeed no one is forgotten.

Last but not least, my greatest debt is to my family for their support, endless patience and encouragement in all forms.

# Abstract

In this work zinc chromate ($ZnCr_2O_4$) samples were produced by hydrothermal and combustion methods. Effect of different synthesis methods upon the structural and optical properties were investigated. X-rays diffraction (XRD) results confirm the formation of the cubic spinel structure with crystallite sizes of 13.8 nm and 23.1 nm for the samples prepared by hydrothermal and combustion methods, respectively. The lattice parameters were calculated using Bragg's law and found to be 8.33 Å and 8.12 Å for the samples prepared by hydrothermal and combustion methods, respectively. The microstrain values were $0.004823 \pm 0.00043054$ and $0.00482 \pm 0.0002738$ for the sample prepared by hydrothermal and combustion methods, respectively. The existence of metal oxide bonds at both samples was confirmed using Fourier transform infrared (FT-IR) spectroscopy technique. The absorption peaks for the $Cr_2O_4$ and Zn-O bonds were observed at 545.074 and 489.3 $cm^{-1}$, respectively for the samples prepared by the hydrothermal method. While in the sample prepared by combustion method the absorption peaks of $Cr_2O_4$ and Zn-O bonds were observed at 545.14 and 489.2 $cm^{-1}$, respectively. The Brunauer–Emmet–Teller (BET) speafic surface area measurements of the sample prepared by the hydrothermal method showed a value of 20.3919 $m^2/g$, while the sample prepared by the combustion method showed a value of 19.81860 $m^2/g$. $N_2$ adsorption-desorption measurements were used to investigate the textural and character of the pores for the synthesized $ZnCr_2O_4$ samples. The optical properties were studied using Ultra violate–visible (Uv-vis) absorption spectroscopic technique. The results show that $ZnCr_2O_4$ samples have a direct band gap of 4.038 eV and 3.98 eV for the samples prepared by hydrothermal and combustion methods, respectively. It observed that the band gap increases as crystallite sizes decrease. It can be concluded that various methods for synthesis $ZnCr_2O_4$ samples lead to different structural properties and significantly affect the optical properties.

# المستخلص


في هذا البحث تم إنتاج عينات لمركب كرومات الزنك بطريقة الإحتراق و الطريقة الحرارية المائية. والهدف من ذلك هو دراسة تأثير طرق التحضير المختلفة علي التركيب و الخصائص الفيزيائية والبصرية للعينات. أكدت نتائج إنحراف الآشعة السينية تكون المادة بحجم بلوري يعادل 13.8 و23.1 نانومتر للعينة المحضرة بالطريقة الحرارية المائية وطريقة الإحتراق، علي التوالي. تم حساب معامل الشبيكة بقانون براغ ووجد انه يساوي 8.33 و8.12 أنجستروم للعينة المحضرة بالطريقة الحرارية المائية وطريقة الإحتراق، علي التوالي. قيم الإجهاد للعينات كانت تساوي 0.00043054 $\pm$ 0.00482 و 0.00043054 $\pm$ 0.004823 للعينة المحضرة بالطريقة الحرارية المائية و طريقة الإحتراق، علي التوالي.

تم التأكد من وجود الروابط المكونة لأكسيد المعدن في كلتا العينتين بواسطة التحليل الطيفي للأشعة تحت الحمراء. وكانت القيم لقمتي الإمتصاص في كل من $Cr_2O_4^{-2}$ و Zn-O تساوي 545.074 و 489.3 سم$^{-1}$ علي التوالي، للعينة المحضرة بالطريقة الحرارية المائية. و كانت القيم لقمتي الإمتصاص $Cr_2O_4^{-2}$ و Zn-O تساوي 545.14 و 489.2 سم$^{-1}$ علي التوالي، للعينة المحضرة بطريقة الإحتراق.

أظهرت دراسات الإمتصاص أن قياسات المساحة النوعية للسطح تبلغ 20.3919 متر$^2$ / جم للعينة المحضرة بالطريقة الحرارية المائية. بينما كانت قيمة مساحة السطح للعينة المحضرة بطريقة الإحتراق 19.81860 متر$^2$ / جم. تمت دراسة طبيعة وخصائص المسامية للعينات عن طريق قياسات الامتزاز والامتصاص للنايتروجين $N_2$.

تمت دراسة الخصائص البصرية عن طريق قياسات الإمتصاص في مدي الأشعة فوق البنفسجية. أظهرت النتائج أن عينات مركب كرومات الزنك تحتوي على فجوة نطاقية مباشرة تساوي 4.038 و 3.98 إلكترون فولت للعينة المحضرة بالطريقة الحرارية المائية و طريقة الإحتراق، علي التوالي. وجد أن قيمة الفجوة النطاقية تقل بزيادة الحجم البلوري للعينات. أكدت النتائج أن الطرق المختلفة في تركيب المادة تؤثر علي خصائص التركيب وتؤدي الي تأثير كبير علي الخواص البصرية.

# Keywords and acronyms

# Keywords

Synthesized, Hydrothermal, Combustion, zinc chromate, optical properties, The Brunauer–Emmet–Teller.

**Acronyms**

Zinc chromate ($ZnCr_2O_4$).

X-rays diffraction (XRD).

Ultra violate –visible (Uv-vis).

Fourier transform infrared spectroscopy (FT-IR).

The Brunauer–Emmet–Teller (BET).

# Table of Contents

**CHAPTER TWO**

**THEORETICAL BACKGROUND**



**CHAPTER THREE**

**EXPERIMENTAL DETAILS**

## CHAPTER FOUR

## RESULTS AND DISCUSSI

# List of figures

# CHAPTER ONE

# INTRODUCTION

## 1.1 General overview

Mineral oxides are typically present in soils comprise oxides, hydroxides, oxyhydroxides and hydrated oxides of Si, Fe, Mn, Al and Ti (Scheinost A.C, 2005). Most of the oxides are formed in soil except Si oxide, quartz and some Ti oxides, which are predominantly inherited from primary (rock) minerals. However, metal cations such as $Si^{4+}$, $Fe^{2+}$, $Mn^{2+}$, $Al^{3+}$ and $Ti^{4+}$ can be obtained naturally from silica (Scheinost A.C, 2005).

Metal oxides are one of the most important and widely characterized solid catalysts (Velmurugan et al, 2018). These oxides are considered as heterogeneous catalysts that can be applied for acid-base and redox reactions. Certain groups of metals, particularly transition metals, have attracted much attention because of their outer electron configuration (Velmuruga et al, 2018). They have been largely applied in a various reactions which includes oxidation, dehydrogenation, dehydration and isomerization. Transitional metal oxides such as $Nb_2O_5$, $WO_3$ (Tagusagawa et al, 2010) and $TiO_2$ (Kondo et al, 2005) are widely used as heterogeneous acid nanocatalysts.

Non-transition metal oxides, such as ZnO and $SnO_2$ have unique optical and electrical properties. These oxides possess a band gap of about 3 eV and s-like conduction band (Ng Y.H et al, 2010). The combination of such properties is highly important for technology that combines light with electronics, which known as transparent optical conductors. The conductivity of these oxides changes easily when they are exposed to oxidizing or reducing gases. This makes ZnO and $SnO_2$ used in chemical sensing and significant candidate in catalysis (Moezzi et al, 2012). Among non-transition metal oxides, $Cr_2O_3$ is considered to be important material that is used in paints, inks, glasses and precursor to the magnetic pigment chromium dioxide. It is also used as a compound for polishing the edges of knives, razors, surfaces of optical devices (Gerd Anger et al, 2005).

Minerals oxides are divided into three categories namely simple oxides, hydroxides and multiple oxides. The characteristic of simple oxides is based on $O^{2-}$ as the main anion and primarily ionic bonding. While, in hydroxides, the dominant anion is the hydroxyl ion $OH^-$.

However, multiple oxides are compounds of two or more metals with oxygen. A major group within this class are the spinels (Dyar, 2008).

### 1.2 Spinel structure

Spinel is an important class of mixed-metal oxides and has the general chemical composition of $AB_2O_4$ where *A* and *B* are cations occupying tetrahedral and octahedral sites, respectively. Normally, *A* is a divalent and *B* is a trivalent atom. The cations occupy only one-eighth of the tetrahedral sites and one-half of the octahedral sites while O designates the oxygen anion position as shown in figure 1.1. The cell units of spinels have their place in the cubic structure (space group F3*dm*) and presented in the cubic form $AOB_2O_3$ by eight molecules and comprising of 32 $O^{-2}$ anions. These oxygen anions from the close face-centered cube (FCC) packing which is contained in 64 tetrahedral (*A*) and 32 octahedral (*B*) empty spaces partially occupied by $B^{3+}$ and $Me^{2+}$ cations. Conferring to the distribution of cations, there are three types of spinel structures, namely normal, mixed and inversed spinels structures. This depends on the point based on which type of ions and the order *A* and *B* in the vacant spaces. In this review, spinel metal chromate has been taken into consideration.

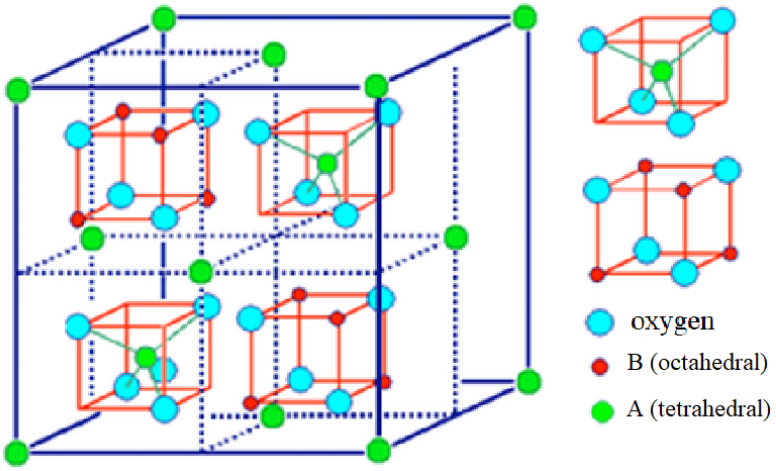


**Figure 1.1**. Graphic representation of two subcells of a spinel structure unit cell, illustrating octahedral and tetrahedral sites.

#### 1.2.1 Normal spinels

In normal spinel structures, all the $Me^{2+}$ ions occupy the *A* sites; the structural formula of such

spinels chromates is $Me^{2+}$ [$Cr_2^3$] $O_4^{2-}$. This type of distribution is observed in spinel zinc chromates $Zn^{2+}$ [$Cr^{2+}Cr^{3+}$] $O_4^{2-}$.

### 1.2.2 Inverse spinels

Inversed spinel structure, in which all the $Me^{2+}$ are in the *B*-site and $Cr^{3+}$ ions are equally dispersed between *A* and *B* sites, the structural formula of these spinel chromates are given by $Cr^{3+}[Me^{2+}Cr^{3+}]$ $O_4^{2-}$. In inversed chromates half of the $Cr^{3+}$ is sited in the *A* sites and the other half in the *B*-sites. The resulting magnetic moment of the chromate is as a result of the magnetic moments of the divalent cations $Me^{2+}$ in the *B* site, the magnetic moments of these types of spinels are mutually compensated.

### 1.2.3 Mixed spinels

In mixed spinel structures, the cations $Me^{2+}$ and $Cr^{3+}$ occupy both *A* and *B* sites, those chromates have a structural formula of $Me_{1-x}^{2+}Cr_x^{3+}$ [$Me_x^{2+}Cr_{2-x}^{3+}$] $O_4^{2-}$, where the degree of inversion is given by *x*.

### 1.2.4 Methods for the synthesis of spinels

Many methods for synthesizing metal oxides spinels have been reported, such as combustion, sol-gel, microwave, hydrothermal, high energy ball milling, micro-emulsion, spray pyrolysis methods. Various types of precipitation agents have been used to achieve specific size and shapes of spinel metal oxides. However, these techniques are found to be more challenging to apply on a larger scale due to their costly and complicated procedures, high temperature of reactions, a lengthy time of reaction, lethal reagents and by-products, and their possibility to cause harm to our immediate environment (Goodarz et al, 2012).

### 1.2.5 Chromates

Transition metal chromates $MCr_2O_4$ (where *M* = Co, Cu, Mn, Ni, and Zn), with spinel structures, have attracted much attention because of their tremendous technological importance as heat resistant pigments, refractories with optical properties, and protective coating materials for interconnects in solid oxide fuel cell stack systems, as well as catalysts for the decomposition of chlorinated organic pollutants. Furthermore, chromates such as $CoCr_2O_4$, $MnCr_2O_4$, and $NiCr_2O_4$

are ferromagnetic spinels; in single-crystal samples, the collinear ferromagnetic ordering occurs at *Tc* = 51 K, 93 K, and 74 K for Mn, Co, and Ni, respectively (Yamasaki et al. 2013).

### 1.2.6 Applications of chromates

Chromates spinels are considered as own one of the most important crystal structures, amongst another spinel structure. Transitional metal chromates which are found throughout the earth's interior, have significant implications on the foundation of a wide range of materials due to their performance at high-pressure conditions. Chromate has been the key raw material in the production of chromium chemicals since the early $19^{th}$ centuries. Chromates are initially used for making bright color pigments. In present days, chromate has been effectively used for the advanced productions of biocides, catalysts, pigments, corrosion inhibitors, chemicals used in oil fields, plating and finishing of metal, tanning compounds and highly pure chromium metal, also used in the production of printing chemicals (White, 2006).

Zinc chromates ($ZnCr_2O_4$) are effective catalyst materials for the synthesis of biodiesel and the removal of methane from compressed natural gas engines and sensor materials. Copper chromate ($CuCr_2O_4$) spinel is one of the most effective catalysts for CO oxidation in automobile-emission control and it also used as a burning catalyst to increase the rates of combustion of solid rocket propellants. It increases the burning rate of propellants at all pressures, producing a good catalytic effect on the decomposition and deflagration rate of ammonium perchlorate and polystyrene solid composite (Gene et al, 2014).

.

### 1.3 Literature review

Several researchers have channeled their efforts to improve and optimize the properties of spinel chromates.

Cheng Peng and Lian Gao (2008) synthesized $ZnCr_2O_4$ samples by hydrothermal method. The experimental results showed that the as-prepared $ZnCr_2O_4$ samples have an average particle size less than 5 nm. The synthesized $ZnCr_2O_4$ samples possessed a direct band gap about 3.46 eV and exhibit blue emission in the range of 300–430 nm, centered at 358 nm when excited at 220 nm. Furthermore, the samples showed apparent photocatalytic activities for the degradation of methylene blue under UV light irradiation (Cheng Peng and Lian Gao, 2008).

Zhongwu Wang et al (2002) used Raman spectroscopic technique to investigate the pressure-induced phase transformation in the synthetic $ZnCr_2O_4$ spinel up to pressures of 70 GPa at room temperature. The results indicated that $ZnCr_2O_4$ spinel starts to transform to the $CaFe_2O_4$ (or $CaTi_2O_4$) structure at 17.5 GPa, and such a phase transformation is complete at 35 GPa (Zhongwu Wang et al, 2002).

Bangale-Bamane (2013**)** studied the electrical properties of $ZnCr_2O_4$ synthesized by combustion method. The synthesized material was characterized by thermos gravimetric differential (TGA) analysis, X-rays diffraction, energy dispersive X-rays microanalysis, and transmission electron microscopy techniques. The increase in conductivity with increasing temperature could be attributed to the negative temperature coefficient of resistance and the semiconducting nature of $ZnCr_2O_4$ **(**Bangale-Bamane, 2013**)**.

Gene-Saion (2014) studied the optical properties of $ZnCr_2O_4$ synthesized by thermal treatment method. The characterization of $ZnCr_2O_4$ nanocrystallite were carried out by X-ray diffraction spectroscopy (XRD), electron dispersive X-ray spectroscopy (EDX), transmission electron microscopy (TEM), Fourier transform infrared spectroscopy (FT-IR), ultra violate –visible (UV-Vis) spectrometer, and electron spin resonance spectroscopy (ESR) (Gene-Saion, 2014).

SumairaNaz (2014) synthesized $ZnCr_2O_4$ by hydrothermal method. $ZnCr_2O_4$ Characterization, phase identification, crystallinity and surface morphology were carried out by x-ray diffraction (XRD) and scanning electron microscopy (SEM). $ZnCr_2O_4$ remained poorly crystallite up to 300$^o$C. Then structure developed after calcination at 600$^o$C for 4h. Formation of single-phase cubic structure confirmed by Rietveld refinement study with lattice parameter 8.2874 Å, Thermal stability of the developed material was observed by thermos gravimetric (TG) and differential thermal analysis (DTA). Thermal study reveals that $ZnCr_2O_4$ is thermally stable above 700$^o$C. The Fourier transform infrared (FT-IR) spectra show the two absorption peaks of Cr-O and Zn-O at 490 and 616 $cm^{-1}$respectively. The band gap energy of $ZnCr_2O_4$ powder using ultra violate-visible (Uv-vis) were 3.771 eV and 3.147 eV for direct and indirect band gap respectively (SumairaNaz et al, 2014).

## 1.4 Problem statement

Spinel materials are attractive subjects of continuous scientific interest and have been deeply investigated in materials sciences. However, structural and optical properties of spinel $ZnCr_2O_4$ samples are expected to be affected by the synthesis method.

## 1.5 Aim of the study

This work aims to investigate the effect of hydrothermal and combustion methods on the structural and optical properties of spinel $ZnCr_2O_4$.

## 1.6 Specific objectives of the study

i. To synthesize spinel zinc chromate samples using the hydrothermal and the combustion methods.
ii. To identify the spinel structure of the synthesized zinc chromate samples by X-rays diffraction technique (XRD).
iii. To refine the XRD results using full proof software in order to obtain the structure parameters.
iv. To study the surface area of the synthesized samples by Brunauer–Emmett–Teller (BET) technique.
v. To investigate the optical properties of the synthesized zinc chromate samples.

## 1.7 Dissertation outline

This dissertation consists of four chapters. Summary of metal oxides in addition to the problem statement, study objectives, a brief discussion on the general background of spinel samples and common methods for synthesis are presented in chapter one. Theoretical background of optical properties and X-rays diffraction spectroscopy are presented in chapter two. The detailes of the synthesis procedures involved of spinel zinc chromate samples by hydrothermal and combustion method are explained in chapter three. Chapter four is devoted to results, discussions, conclusions, recommendations and future work.

# CHAPTER TWO
# THEORETICAL BACKGROUND

This chapter discusses the theoretical background behind the optical properties and the relationship between particle sizes and the optical band gap.

## 2.1 Optical properties

Optical properties (optical absorption and quantum size effect) strongly depend on the size of the particles.

### 2.1.1 Optical absorption

The absorption of the light waves depends on the wavelength of the light, the thickness of the absorber , the transmitted media and the nature of the media. For each wavelength, the intensity of the light passing through the reference cell is measured ($I_o$) and the intensity of the light passing through the sample cell is ($I$). From the Beer Lambert law, the relationship between the absorption ($A$) and the intensities are given by

$$A = log\frac{I_0}{I} = e^{-\alpha x}, \qquad 2.1$$

where $\alpha$ is the absorption coefficient and $x$ is the sample thickness.

Absorption of photons is due to the electronic transitions from the fully occupied outer orbital of metallic composition to the partialy occupied outer orbital of nonmetallic composition. This process can occur over a wide range of photon energies. It involves the absorption of both photons and phonons since both energies and $k$ the energy level, must be changed in the transition (Gene, 2014).

### 2.1.2 Quantum size effect

Distinctive optical properties may arise from another phenomenon known as the quantum size effect. This depends on the size of the particle, especially when the particle size is less than the excitation Bohr radius (the distance in an electron-hole pair) of the material. Excitation Bohr radii are typically on the order of few nanometers for semiconductor samples. As the size of the particles approaches the Bohr excitation radius, the energy level of the samples becomes discrete and quantized. This phenomenon is known as quantum confinement (Rossetti et al, 1982).

At a sufficiently small size of samples, the excitation Bohr radius can become comparable to the crystal dimensions. The excitation wave function cannot extend beyond the edge of the crystal without a severe energetic penalty because of the potential step present at the surface of the crystal. As a result of that, the total excitation wave function will have to be squeezed to fit into the crystal.

This results in an increase in the kinetic energy of the excitation usually called the confinement energy. Due to decreasing particle size, there will be a change in the band structure and so in the properties of the material, in the other hand, as the size of the samples decreases the band gap will increase. Figure 2.1 illustrates the dependence of the band gap on the size of quantum dots.

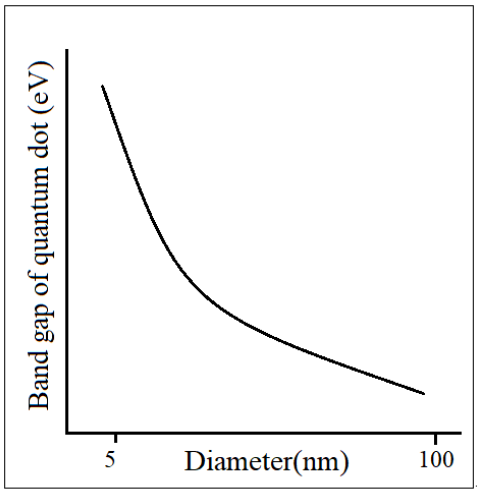


**Figure 2.1**. Schematic illustration of the dependence of band gap to the size of the quantum dot.

An experimental demonstration of the quantum confinement effect is the blue shift of the UV-vis spectrometer with decreasing particle sizes. By employing the particle-in-a-box model of quantum mechanics, the quantum confinement effect may be better described. Similarly, for electronic states, a smaller box will yield a larger energy gap then a larger box. The quantum confinement for spherical particles is given by (Brus, 1984).

$$E_{g,effective(R)} = E_g(\infty) + \frac{h^2\pi^2}{2R^2}\left(\frac{1}{M_e} + \frac{1}{M_h}\right) - \frac{1.8e^2}{\varepsilon R}, \qquad 2.2$$

where $E_g(\infty)$ is the bulk band gap, $M_e$ and $M_h$ are the effective masses of the electron and hole respectively, ε is the bulk optical dielectric constant or relative permittivity and $R$ is the size of the particles.

It could be observed from the second term on the right-hand side of the equation that the effective band gap is inversely proportional to $R^2$ and increases as size decreases. Similarly, the third term indicates that the band gap energy decreases as $R$ decreases due to the increase in columbic interaction. Since the second term is dominant with a smaller value of $R$, the effective band gap is expected to be increasing with a decrease in the value of $R$, particularly when $R$ is small. Figure 2.1 illustrates this effect, the influence of solvent is typically small compared to quantum confinement, so is neglected from this form of the equation.

### 2.2 Optical band gap

The band gap energy can be determined from the absorption coefficient constant $\alpha(v)$, which depends on the frequency of the UV spectrum (Tauc, 1974),

$$\alpha(v)hv = B(hv - E_g)^m, \qquad 2.3$$

where $hv$ is the incident photon energy, $h$ is the Planck constant, $E_g$ is optical band gap energy and $B$ is the disorder parameter constant which is depends on the composite compositions , independent to the photon bonding and $m$ is the power coefficient with the value that can be determined by the types of possible electronic transitions, $n$ = 1/2 for allowed direct (Hagfeldt, 1995), $n$ = 1 for allowed indirect, $n$ = 3/2 for forbidden direct and $n$ = 2 for forbidden indirect (Li et al, 2006). In direct allowed transitions, the electrons are transferred directly from the valance band to the conduction band by the transition-dipole moments and the electric fields at the surface, while in indirect allowed transitions, the incident photon is absorbed which is then followed by scattering of photo-excited electron trapped in the intermediate state and then transferred to the conduction band. Electrons of the valance band can be connected to the empty states in the conduction band by indirect transition process. Nevertheless, phonons could also take part in the transition process (Tauc, 1974).

## 2.3 X-rays diffraction spectroscopy (XRD)

The interaction of the incident X-rays with the sample produces constructive interference when Bragg's Law is satisfied. The diffracted X-rays are then detected, processed and counted. By scanning the sample through a range of $2\theta$ angles, all possible diffraction directions of the lattice can be attained. Figure 2.2 shows the interference pattern of X-rays scattered by a crystal.

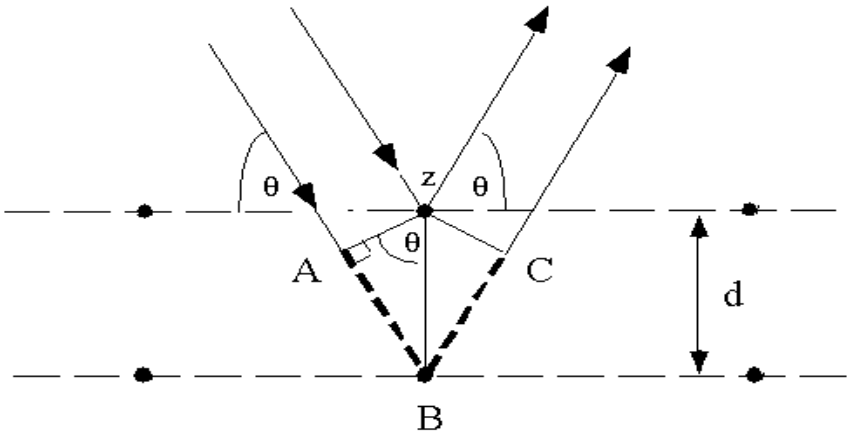


**Figure 2.2**. The interference pattern of X-rays scattered by a crystal**.**

The crystallite sizes can be obtained using Scherer's equation

$$D = K\lambda/(\beta \cos \theta), \qquad 2.4$$

where $D$ is the mean sizes of the ordered domains (crystallite sizes), which may be less or equal to the grain sizes, $K$ is a dimensionless shape factor with a value close to unity with a typical value of about 0.9, $\lambda$ is the X-rays wavelength and $\beta$ is the full width half maximum intensity (FWHM) and $\theta$ is the Bragg angle.

Lattice parameter refers to the physical dimension of uniting cells in a crystal lattice. Lattices in three dimensions generally have three lattice constants, referred to *a*, *b*, and *c*. However, in the special case of cubic crystal structures, all of the constants are equal and only referred to *a*.

The lattice parameters were calculated from the XRD spectra using the equation

$$a = \frac{\lambda}{2 \sin \theta} (h^2, k^2, l^2)^{\frac{1}{2}}, \qquad 2.5$$

where $a$ is the lattice parameter in angstrom, $\lambda$ is the X-rays wavelength, $\theta$ is the Bragg angle, $h$, $k$, and $\ell$ are Miller indices.

X-rays densities $\rho_{XRD}$ of a sample can be estimated by using the relation that suggested by Smith and Wijn,

$$\rho_{XRD} = 8M_0/N_A a^3, \qquad 2.6$$

where $M_0$ is the molecular weight, $a^3$ is the volume of the unit cell and $N_A$ is the Avogadro's number.

The microstrain values can be calculated using the equation suggested by willimson-hall,

$$\varepsilon = \beta/4\tan\theta\,, \qquad 2.7$$

where $\varepsilon$ is the microstrain.

# CHAPTER THREE
# EXPERIMENTAL DETAILS

This chapter provides information about synthesis methods, instruments and experimental procedures that were used in this work.

## 3.1 Synthesis methods

Wet chemical synthesis methods such as combustion and hydrothermal are wildly used in synthesizing materials. The main feature of these methods is producing mono-dispersive particles. Metal chlorides or nitrate are commonly used as starting materials. In this work zinc chromate ($ZnCr_2O_4$) samples were synthesized by two different methods namely hydrothermal and combustion methods.

### 3.1.1 Hydrothermal method

Hydrothermal is known as low-temperature synthesis technique for producing materials. The basic principle of this synthesis method depends on the solubility of metal chlorides or nitrates in hot water in a closed system. The advantages of the hydrothermal synthesis method include the ability to synthesize crystals of substances which are unstable near the melting point and also producing crystals with high quality. However, it has some drawbacks of this synthesis method include relatively high cost of equipment.

$ZnCr_2O_4$ sample was prepared by dissolving 3.97 g of Zn $(NO_3)_2.6H_2O$ and 10.50 g of Cr $(NO_3)_3$ $.9H_2O$ in 50 mL of deionized water to form a clear aqueous solution. NaOH solution was slowly dropped into the mixed solution, vigorously stirred to adjust the pH from 4 to 9.01. The obtained suspension of the mixed solution was stirred for 30 mins at speed 3rps. The solution was placed in the centrifuge device for 3 mins at 60 rpm. The hydrothermal reaction was conducted refluxing the mixuter at 100 ºC for 20 h in the mantle heater. After the reaction completed, the product was collected by filtraition and then washed with Ethanol two times. Finally, pale gray powder was obtained after being dried in an oven at 60 ºC for 2h. Figure 3.1 show the experimental set up of the hydrothermal method.

### 3.1.2 Combustion method

The combustion method is considered to be an effective and low-cost synthesis technique.

In this method, a fuel such as urea is needed which possesses a high heat of combustion.

**Figure 3.1**. Experimental set up of the hydrothermal method, Chemistry laboratory, Africa City of Technology.

It is an organic fuel providing a platform for redox reactions during the course of combustion (Bangale et al, 2011).

$ZnCr_2O_4$ sample was prepared by dissolving 3.9g Zn $(NO_3)_2.6H_2O$, 10.97g Cr $(NO_3)_2.9H_2O$ and 5.19 g of urea in 50 mL of deionized water to form a clear aqueous solution. The paste formed was evaporated on a hot plate at 70 ºC until a thick gel was obtained. The temperature was raised up to 250 ºC for the auto combustion reaction. The final powder obtained was a pale green color. Figure 3.2 shows the experimental set up of the combustion method.

**Figure 3.2.** Experimental set up of the combustion method, chemistry laboratory, Africa City of Technology.

### 3.2 Characterization techniques

The synthesized $ZnCr_2O_4$ samples were characterized using X-rays diffraction spectroscopy (XRD), Fourier transform infrared spectroscopy (FT-IR), Brunauer, Emmett and Teller (BET) surface area measurements, and ultraviolet-visible spectroscopy (UV-vis).

#### 3.2.1 X-rays diffraction spectroscopy

X-rays diffraction (XRD) is an analytical technique mainly used for phase identification of crystallite materials. When a parallel beam of monochromatic X-rays is irradiated on a sample, the atomic lattice of the sample acts as a three-dimensional diffraction grating causing the X-rays beam to be diffracted to specific angles. The results obtained from XRD measurements give information about the investigated sample such as lattice parameters, crystallite sizes, and microstrain.

The structural characterization of the synthesized spinel zinc chromate samples was performed by the Shimadzu diffractometer (Model XRD 6000) with Cukα (0.154 nm) radiation source over the $2\theta$ range of 10° to 80°. Figure 3.3 shows the X-ray diffractometer.


**Figure 3.3**. The X-rays diffractometer King Fahad for Minerals and Petroleum University, Saudi Arabia.

### 3.2.2 Fourier transform Infrared (FT-IR) Spectroscopy

The principle of Fourier transforms infrared (FT-IR) is based on the molecular bonds vibration at various frequencies. This depends on the elements and the type of bonds. There are several specific frequencies at which any given bond can vibrate. These frequencies correspond to the ground state (lowest frequency) and several excited states (higher frequencies).

Absorption of light energy is used to increase the vibration of the frequency of a molecular. The energy corresponding to the transition between molecular vibrational states is ranging between 1-10 kilocalories/mole. This corresponds to the infrared (IR) portion of the electromagnetic spectrum. As shown in figure 3.4 the basic components of IR include a source, collimator, beam splitter (mirror), fixed mirror, moving mirror, sample compartment, laser for aligning the mirrors as well as for internal calibration and detector. Figure 3.5 shows fourier transforms Infrared (FT-IR) Spectrometer.

Infrared spectra were recorded using Fourier transform infrared (FT-IR) spectrometer (Perkin Elmer model 1650) in the wave number range between 480 - 4000 $cm^{-1}$.

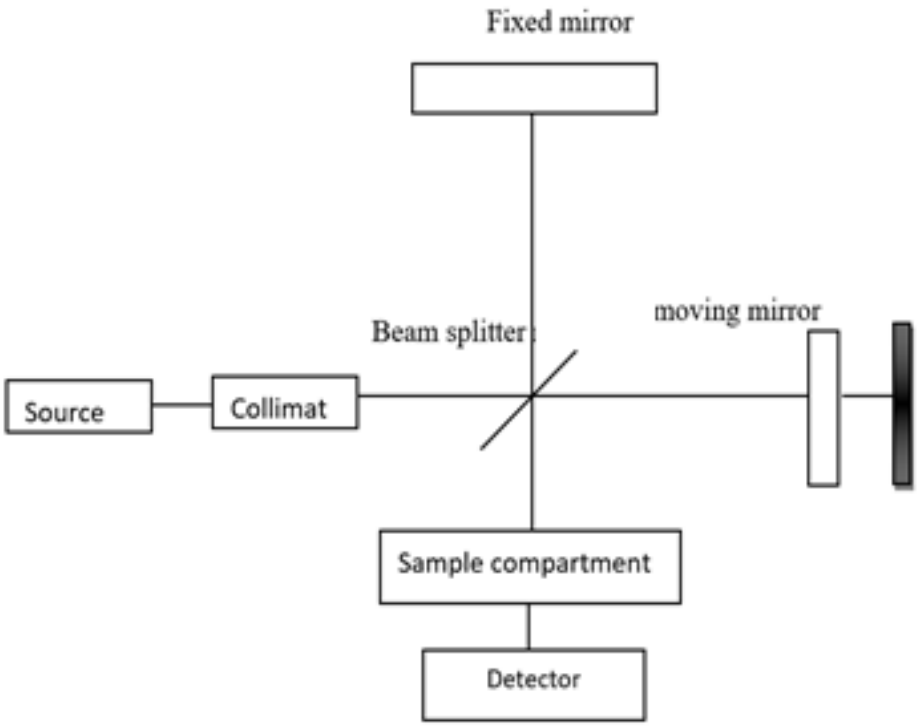


**Figure 3.4.** Schematic diagram of the IR instrument.

**Figure 3.5.** Fourier transforms Infrared (FT-IR) Spectrometer, Sudan University of Science and Technology, Sudan**.**

### 3.2.3 Brunauer–Emmett–Teller (BET) measurements

Brunauer Emmett Teller(BET) surface area measurements is a technique to calculate the specific surface area and pore sizes distribution of a sample. As shown in figure 3.6 the volume of gas (usualy nitrogen) adsorbed to the surface of the particles is measured at the boiling point of nitrogen (-196°C). At this temperature, the nitrogen gas is below the critical temperature and so condenses on the surface of the particles. It is assumed that the gas condenses into the surface in a monolayer, since the size of the gas atom/molecule is known, the amount of adsorbed (condensed) gas is correlated to the total surface area of the particles including pores at the surface (inaccessible pores are not detected). Figure 3.7 shows the Brunauer–Emmett–Teller (BET) surface area analyzer.

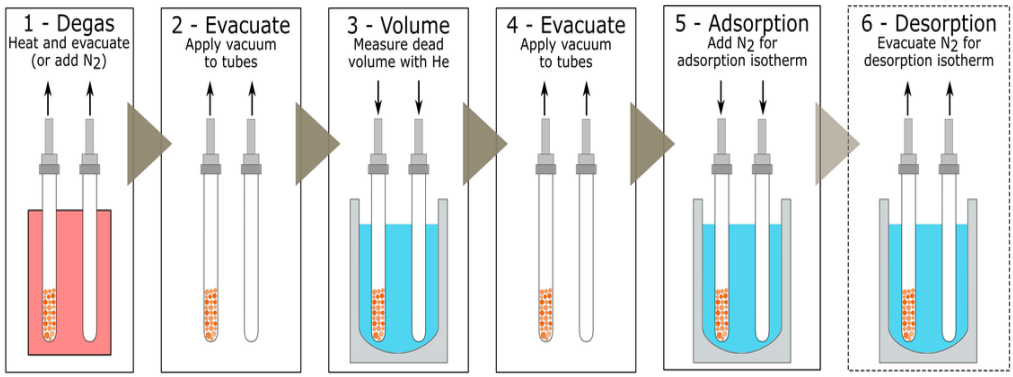


**Figure 3.6.** Schematic diagram of measuring surface area with BET.

**Figure 3.7.** The Brunauer–Emmett–Teller (BET) surface area analyzer King Fahad for Minerals and Petroleum University, Saudi Arabia.

### 3.2.4 Ultraviolet-visible spectroscopy

Ultraviolet-visible (UV-visible) spectroscopy principle is described in figure 3.8, in which a beam of light from a UV-visible light source is separated into its component wavelengths by a diffraction grating. Each monochromatic beam splits into two equal intensity beams by a half-mirrored device. One beam (colored magenta) passes through a small transparent container (cuvette) as a sample chamber. The other beam uses as a reference (colored blue) passes through an identical cuvette. The intensities of these light beams are then measured by electronic detectors and compared. The intensities of the reference and sample beams are denoted as $I_0$ and $I$ respectively.

The scanned UV region is normally from 200 to 400 nm, and the visible portion is from 400 to 800 nm (Whiffen, 1971). In the case of the sample does not absorb the light of a given wavelength, then $I = I_0$.

However, if the sample absorbs the light then $I$ is less than $I_0$. Absorption may be presented as transmittance ($T = I/I_0$) or absorbance ($A = log\ I_0/I$). If no absorption occurred, then $T$ takes a value of 1.0 and $A$ is 0.

Most spectrometers display absorbance on the vertical axis, and the commonly observed range is from 0 (100% transmittance) to 2 (1% transmittance). The wavelength of maximum absorbance is a characteristic value, designated as $\lambda$ max. Figure 3.9 shows the ultra-violet- visible (UV-Vis) spectrometer.

The reference absorption intensity for the system is based on a completely transparent standard compound (non-absorbing).

The most commonly used compounds are water, ethanol, hexane and cyclohexane. The compounds with double or triple bonds and heavy atoms are generally avoided because the absorbance of a sample is proportional to its molar concentration in the sample cuvette.

In this study, the optical properties of the synthesized spinel zinc chromite powders were studied using the ultraviolet-visible spectrometer (UV-vis) model (SPUV 26). The optical absorbance of the samples was recorded in a wavelength range between 200 to 800 nm.

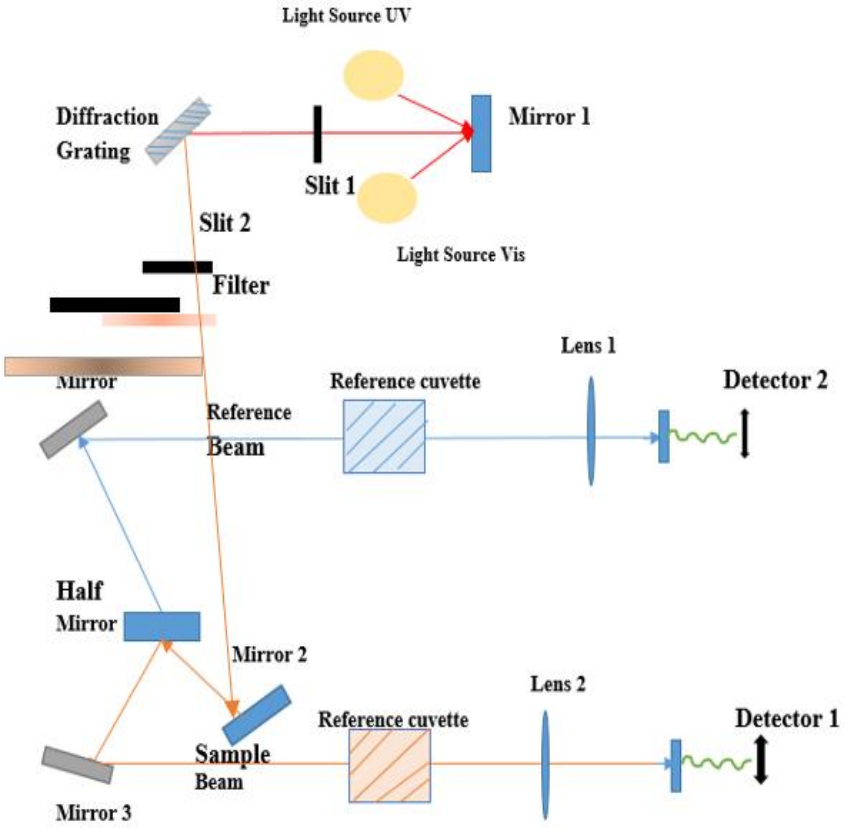


**Figure 3.8.** The schematic diagram illustrated the principle of UV-visible spectroscopy (Smith, 1978).


**Figure 3.9.** The ultra-violet- visible (UV-Vis) spectrometer, Sudan University of Science and Technology, Sudan.

# CHAPTER FOUR
# RESULTS AND DISCUSSION

This chapter devotes to present and discuss the structural and optical properties of spinel zinc chromate ($ZnCr_2O_4$) samples synthesized by hydrothermal and combustion methods.

## 4.1 X-rays diffraction results of the synthesized zinc chromate ($ZnCr_2O_4$) samples

The crystallite phase of the zinc chromate samples was identified using the X-rays diffraction (XRD) spectroscopy. The XRD data were collected in the $2\theta$ range of $10° < 2\theta < 80°$ using CuKα as X-rays source with wavelength λ 0.154 nm. The two samples show the reflection planes of (111), (220), (311), (222), (400), (422), (511), (440), (533) and (622) as shown in figure 4.1, which are characteristics of single-phase cubic spinel structure with space group F*d*-3m (Manikandan.A, 2013). The lattice parameters (*a*) were calculated from the XRD data using equation 2.5. The calculated lattice parameters were 8.33 Å and 8.12 Å for the sample prepared by hydrothermal and combustion methods, respectively. The variation in lattice parameters values is associated with the change in the crystallite sizes in the samples. The XRD patterns of the samples were fitted using the Rietveld program full proof as shown in figure 4.1 the difference between the experimental data and the refinement in the lattice parameters were 0.009 Å, and 0.02091 Å for the sample prepared by hydrothermal and combustion methods, respectively. This difference between the experimental data and the refinement in the lattice parameters could be due to the background on the X-rays patterns which may affect the fitting processes. Since no additional phase was observed, hence, the obtained results are in agreement with the JPCDS standard card no 96-900-3704.

The average crystallite sizes (*D*) were determined using Scherer's formula as in equation 2.4.

The calculated values of crystallite sizes were 13.8 nm and 23.1 nm for the sample prepared by hydrothermal and combustion methods, respectively. The crystallite sizes increase as the synthesis temperature increases due to the centering effect (Houshiar et al.,2014).

The X-rays densities ($\rho_{XRD}$) of the synthesized $ZnCr_2O_4$ samples were determined using equation 2.6. The calculated values were 3.275 g/cm$^3$ and 3.499 g/cm$^3$ for the sample prepared by the hydrothermal and combustion methods, respectively. The variation in the values of X-rays densities is associated with the difference in lattice parameters of the samples.

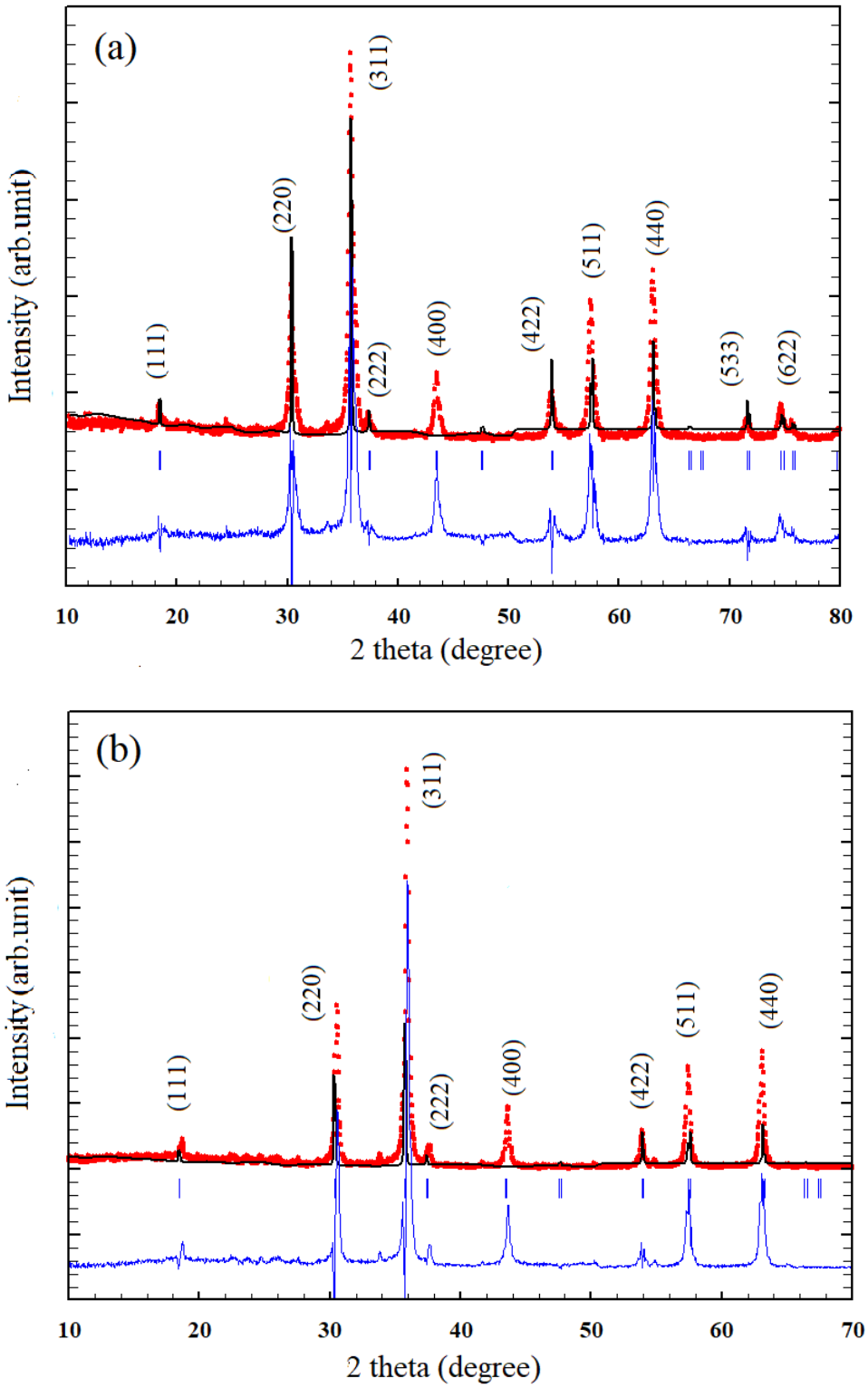


**Figure 4.1.** XRD patterns of $ZnCr_2O_4$ samples prepared by (a) hydrothermal and (b) combustion methods.

The microstrain ($\varepsilon$) values were calculated using equation 2.7. The obtained values were $0.004823 \pm 0.00043054$ and $0.00482 \pm 0.0002738$ for the sample prepared by hydrothermal and combustion methods, respectively.

The variation in microstrain values is associated with the change in synthesis temperature.

Since the reaction temperature of the combustion method was higher compared to the hydrothermal method. Therefore, the sample prepared by the combustion method was expected to have less value of microstrain.

**4.2 FT-IR spectra of zinc chromate ($ZnCr_2O_4$) samples**

The functional groups of the zinc chromate samples were identified using the Fourier transform infrared (FT-IR) spectroscopy. Figure 4.2 shows the FT-IR spectrum of zinc chromate sample prepared by hydrothermal method. The peak at 1339.6 $cm^{-1}$ is associated with C-N vibration from the Amine group, the appearance of the peak at 1644.4 $cm^{-1}$ is attributed to C=C stretch vibration from the Alkene group, while the peak at 1400.9 $cm^{-1}$ is associated with C-H bending vibration from the methylene group, the peak 3455.9 $cm^{-1}$which is associated with vibration N-H bending vibration from the Amine group. The absorption peak of Zn-O bond is observed at 489.3 $cm^{-1}$. The absorption peak of the chromium $Cr_2O_4$ is observed at 545.074 $cm^{-1}$ (Loria et al, 2011).

Figure 4.3 shows the FT-IR spectrum of zinc chromate sample prepared by combustion method. The peak at 1338.7 $cm^{-1}$ was associated with C-N stretching vibrations from the Amine group, while the peak at 1400.2 $cm^{-1}$ was associated with C-H bending vibration methylene group, the appearance of the bands at 1501.05 and 1643.94 $cm^{-1}$ were attributed to C=C stretching vibrations from the alkenes group, the band 3414.37 $cm^{-1}$ was associated with N-H bending vibrations from the Amine group, and the absorption bands of $Cr_2O_4$ and Zn-O bonds were observed at 545.14 and 489.2 $cm^{-1}$ respectively (Loria et al., 2011).

The FT-IR data were collected in the range of 480 - 4000 $cm^{-1}$, the samples show the presence of two principle absorption peaks of $Cr_2O_4$ and Zn-O. The IR peaks in ranges between 600-480 $cm^{-1}$ which are characteristic vibration band for $Cr_2O_4$ bonds of chromium atoms in the tetragonal and octahedral environment of the oxygen atom could be attributed to the chromate samples (Shyuada, 2013).

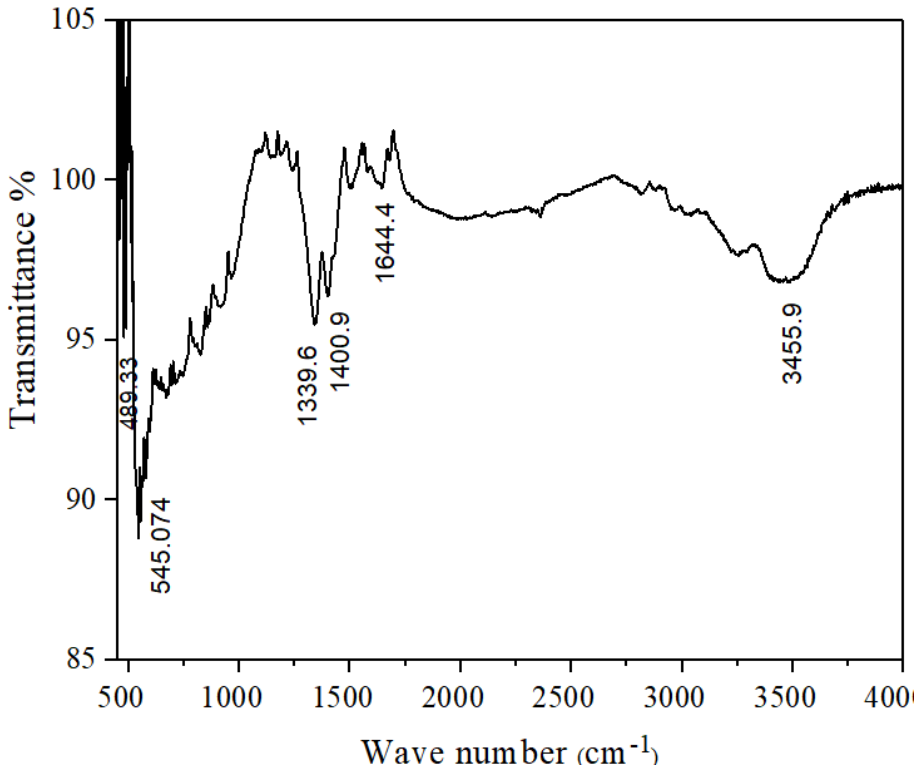


**Figure 4.2** FT-IR spectra of $ZnCr_2O_4$ sample prepared by the hydrothermal method.

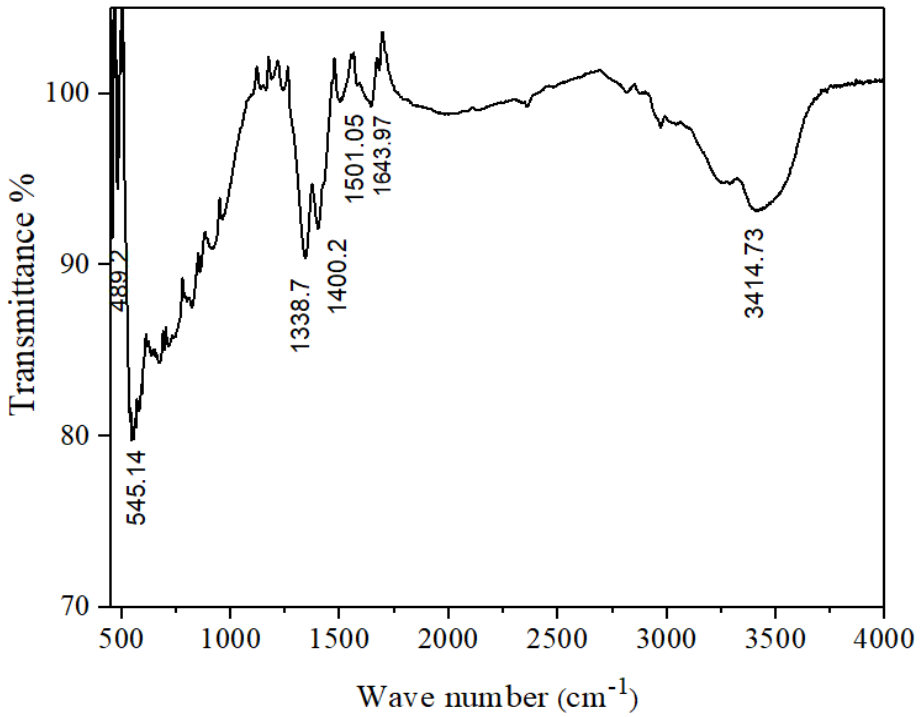


**Figure 4.3.** FT-IR spectra of $ZnCr_2O_4$ sample prepared by the combustion method.

### 4.3 Brunauer, Emmett, and Teller (BET) measurements

The surface area measurements and the porosity of the zinc chromate samples were identified using the Brunauer, Emmett, and Teller (BET) technique. Figure 4.4 shows the $N_2$ gas adsorption isotherms for the $ZnCr_2O_4$ samples prepared by hydrothermal and combustion methods. surface area measurements showed a value of 20.3919 and 19.81860 $m^2/g$ for the $ZnCr_2O_4$ sample synthesized by hydrothermal and combustion method, respectively. $N_2$ adsorption-desorption measurement was used to investigate the textural and character of the pores.

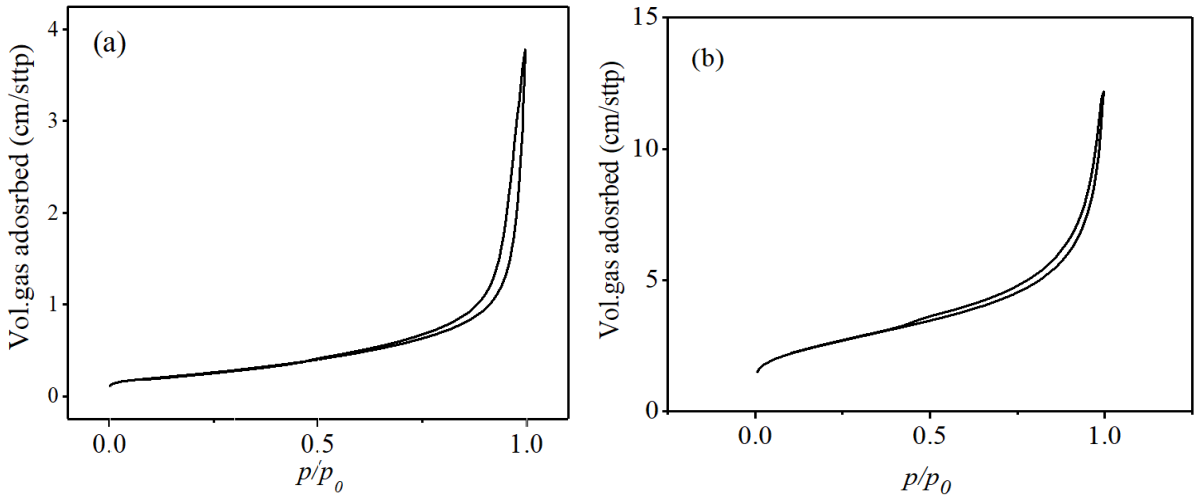


**Figure 4.4.** $N_2$ Gas adsorption isotherms for the $ZnCr_2O_4$ prepared by (a) hydrothermal and (b) combustion methods.

At a relative pressure $P/P_0$ of 0.133 %, the adsorption of $N_2$ increased from 0.1068 $cm^3/g$ to reach its maximum value of 3.778 $cm^3/g$ at $P/P_0$ of 100 %, for the sample prepared by hydrothermal method and for the sample prepared by combustion method $P/P_0$ of 0.6%, the adsorption of $N_2$ increased from 1.44 $cm^3/g$ to reach its maximum value of 12.14 $cm^3/g$ at $P/P_0$ of 100 %.

The distribution of the pores in the sample was investigated by Barrett–Joyner–Halenda (BJH) measurements, as shown in Figure 4.5, the pore diameter was 36.339 $cm^3/g$ and 35.365 $cm^3/g$ for the sample prepared by hydrothermal and combustion methods, respectively.
Which strongly hints towards mesoporous property of the two samples (Lihitkar et al, 2012). Additionally, the sharpness of the peak indicated homogenous porosity of the samples.

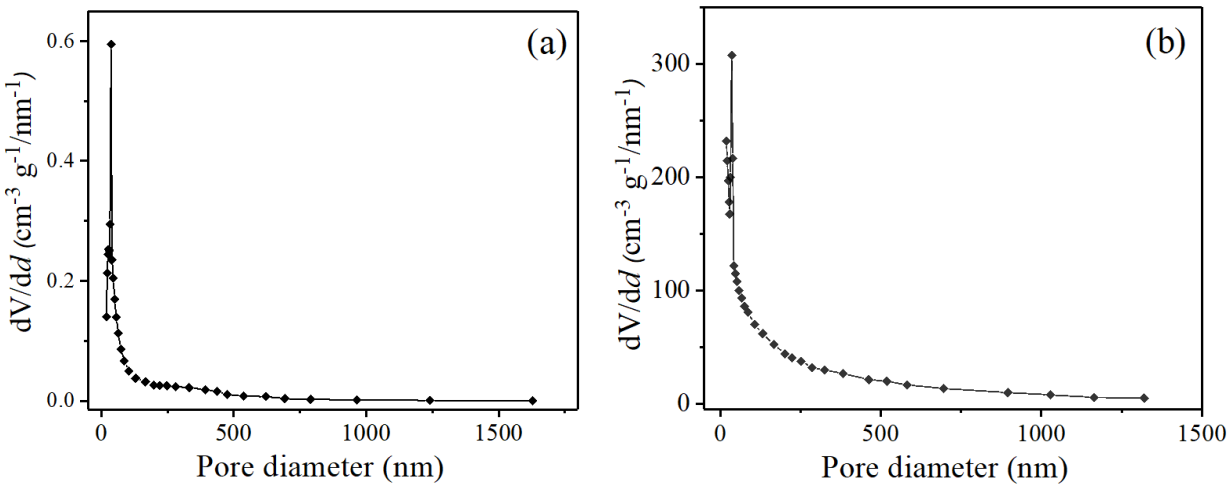


**Figure 4.5.** The pore sizes distribution for the $ZnCr_2O_4$ prepared by (a) hydrothermal and (b) combustion methods.

### 4.4 Uv-vis absorption results of $ZnCr_2O_4$ samples

The optical band gap of the synthesized zinc chromates samples was determined by ultraviolet-visible (Uv-vis) absorption technique. The optical absorption spectrum of the studied $ZnCr_2O_4$ samples shows absorption peaks in the UV range as displayed in figure 4.6. The prominent peak in the UV region could be attributed to band gap absorption of the $ZnCr_2O_4$ samples. The optical band gap ($E_g$) of synthesized samples can be calculated using the optical absorption spectrum based on the equation

$$(Ah\upsilon)^n = B(h\upsilon - Eg) \qquad 4.1,$$

where $h\upsilon$ is the photo-energy, $A$ is absorbance, $B$ is a constant relative to the material when $n$ depends on whether the transition is direct ($n$ = 2) or indirect ($n$ = 1/2), The optical band gap for the absorption peak can thus be deducted by extrapolating the linear portion of the $(Ah\upsilon)^2$ vs $h\upsilon$ curve to zero. As seen in figure 4.7 no linear relation was observed from the function curve of $(Ah\upsilon)^2$ vs $h\upsilon$.This indicates that the as-prepared $ZnCr_2O_4$ samples possess a direct optical band gap.

The calculated band gaps were 4.038 eV and 3.98 eV for the samples prepared by hydrothermal and combustion methods, respectively.

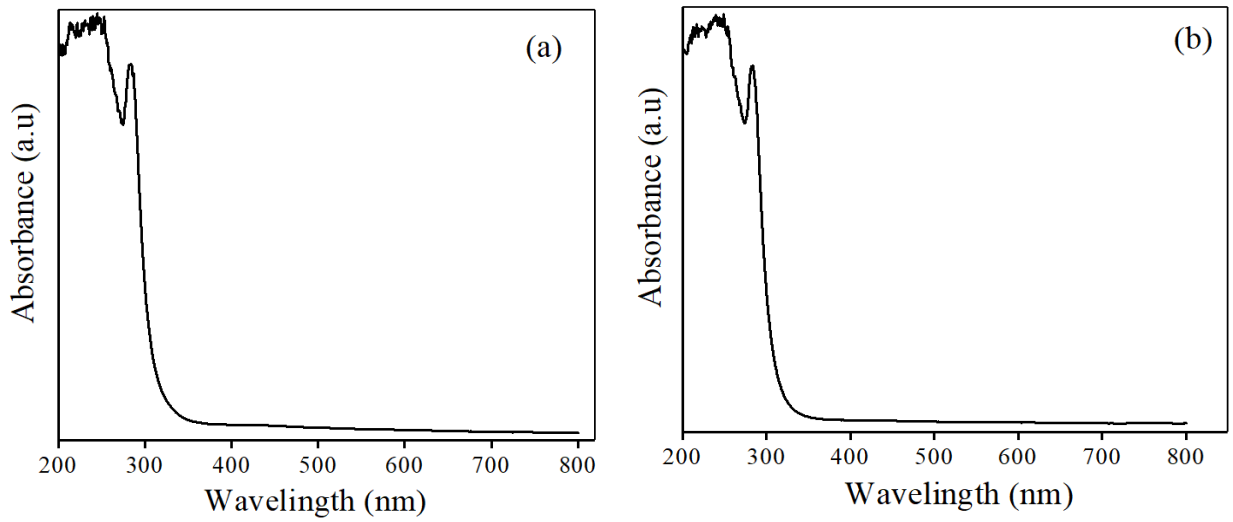


**Figure 4.6.** Uv-vis absorption spectrum of $ZnCr_2O_4$ prepared by (a) hydrothermal and (b) combustion methods.

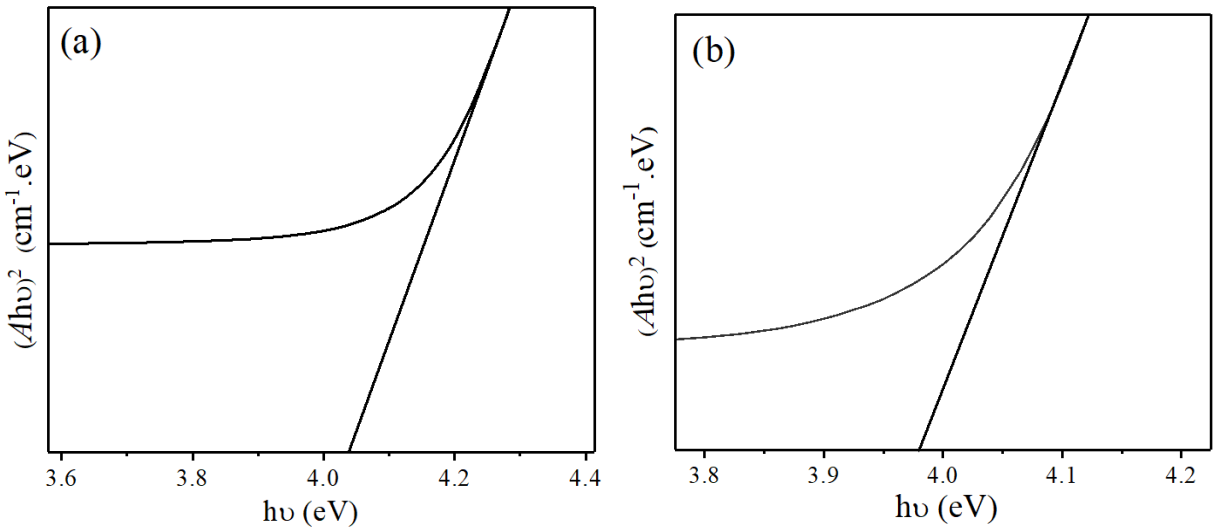


**Figure 4.7.** The $(Ah\upsilon)^2$ vs $h\upsilon$ curve of $ZnCr_2O_4$ samples prepared by (a) hydrothermal and (b) combustion methods.

The energy band gap of the sample prepared by the hydrothermal method was greater compared to the sample prepared by the combustion method.This can be attributed to the higher temperature of the combustion reaction which increases the crystallite sizes. The effect of crystallite sizes on the band gap of a material can be explained based on the quantum size effect (Bhargava et al, 2010).

## 4.5 Conclusions

Spinel zinc chromate ($ZnCr_2O_4$) samples were successfully synthesized by hydrothermal and combustion methods. The influence of the different synthesis methods on the structural and optical properties of $ZnCr_2O_4$ samples was investigated.

The formation of cubic single phase of the zinc chromate samples was identified using the X-rays diffraction spectroscopy. The XRD patterns show that the synthesized samples are well crystalline.

The average crystallite sizes were 13.8 nm for the sample prepared by hydrothermal method and 23.1 nm for the sample prepared by combustion method.

Fourier transform infrared (FT-IR) measurements show that the absorption peaks for the $Cr_2O_4$ and Zn-O bonds were at 545.074 and 489.3 $cm^{-1}$ for the sample prepared by the hydrothermal method, respectively. While for the sample prepared by combustion method the absorption peaks of $Cr_2O_4$ and Zn-O bonds were observed at 545.14 and 489.2 $cm^{-1}$, respectively. This support the results obtined by XRD measurements.

Surface area measurements of the sample synthesized by hydrothermal method was 20.3919 $m^2/g$ and 19.81860 $m^2/g$ for the sample synthesized by combustion method. Barrett–Joyner–Halenda (BJH) measurements shows that the pore diameters are 36.339 $cm^3/g$ and 35.365 $cm^3/g$ for the sample prepared by the hydrothermal and the combustion methods, respectively. The results confirm that the produced samples possess a mesoporose property.

Ultraviolet-visible (UV-vis) measurements show that the prepared $ZnCr_2O_4$ samples possess a direct optical band gap. The calculated band gap for the sample prepared by hydrothermal method is 4.038 eV and 3.98 eV for the sample prepared by combustion method. It observed that the band gap increases as crystallite sizes decrease. The structural and optical properties of the synthesized spinel $ZnCr_2O_4$ samples were significantly affected by synthesis methods.

## 4.6 Recommendations

In light of this study, some recommendation can be suggested which may lead to the best results for a similar study

- Additional information about structure can be obtained from full proof such as atoms position and molecule bonding.

- The average particle sizes of the synthezied samples can be to obained from transmission electron microcopy (TEM).
- Surface morphology of the synthezied samples can be investigated using scanning electron microsopy (SEM).

**4.7 Future work**

This simple, cost-effective, and environmentally-friendly method, which has low reaction temperatures and produces no by-product effluents, can be used to fabricate pure spinel $ZnCr_2O_4$ samples. For any advanced study, the following features should be considered, so as to contribute a new finding of interest as well as to understand the new properties of other transitional metal chromates samples.

- $ZnCr_2O_4$ samples can be prepared using other synthesis methods such as sol-gel, microwave, ball milling, micro-emulsion.
- Effect of annealing treatment on structural and opteical properties of $ZnCr_2O_4$ samples can be investigated.
- Magnetic properties of $ZnCr_2O_4$ samples can be studied using vibrating sample magnetometer (VSM).

## REFERENCES


Abdulsattar, Mudar A. (2011). "Ab initio large unit cell calculations of the electronic structure of diamond samples". Solid State Sci.13: 843.Bibcode:2011Sci.13.843A. doi:10.1016.solidstatesciences.2011.03.009.

Atwater, H. A. (1962). Introduction to microwave theory. McGraw-Hill. Bandaru, P. R., Chiara D., Sungho J., and Rao A. M. (2005). "Novel Electrical Switching Behavior and Logic in Carbon Nanotube Y-Junctions." Nature Materials 4 (9): 663-666.

Bangale, S. V., and Sambhaji R. B. (2011). "Preparation, Wettability and Electrical Properties of Nanocrystallite $ZnCr_2O_4$ Oxide by Combustion Route." Archives of Applied Science Research 3, no. 4(3):300-308.

Bhargava, R., Prashant K. S., Amit K. C., Sanjeev K., Ramesh C., Avinash C. P., and Naresh K. (2011). "Variation in Structural, Optical and Magnetic Properties of $Zn_{1-x}Cr_xO_x$= 0.0, 0.10, 0.15, and 0.20) Samples: Role of Dopant Concentration on Non-Saturation of Magnetization." Materials Chemistry and Physics 125 (3): 664-671.

Brunauer, Emmett, Teller Adsorption of Gases in Multimolecular Layers, Feb (1938), 60, 309.

Brus, L. E. (1984). Electron-electron and electron-hole interactions in small semiconductor crystallites: The size dependence of the lowest excited electronic state. The Journal of chemical physics, 80(9), 4403-4409.

Chen, Z., Shi, E., Zheng, Y., Li, W., Wu, N., & Zhong, W. (2002). Synthesis of mono-dispersed $ZnAl_2O_4$ powders under hydrothermal conditions. Materials Letters, 56(4), 601-605.

Determination of the specific surface area of solids by gas adsorption — BET method, second edition, BS ISO 9277:2010 doi:10.1002/14356007.a07_067.

Dyar, M.D.; Gunter, M.E. (2008). Mineralogy and Optical Mineralogy. Chantilly, VA: Mineralogical Society of America. ISBN 978-0939950812.

Gene, S.A., Saion, E., Shaari, A.H., Kamarudin, M.A., Al-Hada, N.M. and Kharazmi, A., (2014). Structural, optical, and magnetic characterization of spinel zinc chromite nanocrystallinessynthesised by thermal treatment method. Journal of Nanomaterials, p.15

Gerd Anger, Jost Halstenberg, Klaus Hochgeschwender, Christoph Scherhag, Ulrich Korallus, Herbert Knopf, Peter Schmidt, Manfred Ohlinger, "Chromium Compounds" in Ullmann's

Goodarz N. M., Elias B. S., and Ahmad K.i. (2012). "An Overview on Nanocrystallite $ZnFe_2O_4$, $MnFe_2O_4$, and $CoFe_2O_4$ Synthesized by a Thermal Treatment Method." ISRN Nanotechnology no 11.

Hagfeldt and M. Graetzel, (1995) ‘‘Light-Induced Redox Reactions in nanocrystallite Systems,’’ Chem. Rev., no (95), 49–68.

Jenkins, A., & Stephens, P. W. (1991). U.S. Patent No. 5,00-,072. Washington, DC: U.S. Patent and Trademark Office.

Kondo, S., Kittikorn, M. and Kanlayanarat, S., (2005). Preharvest antioxidant activities of tropical fruit and the effect of low temperature storage on antioxidants and jasmonates. Postharvest Biology and Technology, no 36(3), pp.309-318.

Krusin-E. L., Newns D. M, Zeng H., Derycke V., Sun J. Z., and Sandstrom R. (2004). "Room-Temperature Ferromagnetic Nanotubes Controlled by Electron or Hole Doping." Nature 431, no. (7009): 672-76.

Lao, J.Y., Huang, J.Y., Wang, D.Z. and Ren, Z.F., (2003). ZnO nanobridges and nanonails. Nano Letters, no 3(2), pp.235-238.

Li, X. Zhang, Z. Li, and Y. Qian, (2006) ‘‘Synthesis and Characteristics of NiO Samples by Thermal Decomposition of Nickel Dimethylglyoximate Rods,’’ Solid State Commun, no (137), 581–4.

Lihitkar, P.B., Violet, S., Shirolkar, M., Singh, J., Srivastava, O.N., Naik, R.H. and Kulkarni, S.K., (2012). Confinement of zinc oxide samples in ordered mesoporous silica MCM-41. Materials Chemistry and Physics, no 133(2-3), pp.850-856.

Loría-Bastarrachea, M. I., Herrera, K. W., Cauich-Rodríguez J.V., Cervantes-Uc, J.M., Vázquez, T. H., and Ávila, O. A. (2011). "A Tg/FT-IR Study on the Thermal Degradation of Poly (Vinyl Pyrrolidone)." Journal of thermal analysis and calorimetry 104 (2): 737-742.

Manikandan, A., Vijaya, J.J., Kennedy, L.J. and Bououdina, M., (2013). Structural, optical and magnetic properties of $Zn_{1-x}Cu_xFe_2O_4$ samples prepared by microwave combustion method. Journal of molecular structure, 1035, pp.332-340.

McNaught and A. Wilkinson, ed. (1997). IUPAC Compendium of Chemical Terminology the goldbook 2.3.3(2nde).Oxford:Black well scientific UK doi:10.1351/goldbook.S05806. ISBN 0-9678550-9-8l.

Moezzi, Amir; McDonagh, Andrew M.; Cortie, Michael B. (2012). "Review: Zinc oxide particles: Synthesis, properties and applications". Chemical Engineering Journal. 185–186: 1–22.

Ng, Y.H., Iwase, A., Kudo, A. and Amal, R., (2010). Reducing graphene oxide on a visible-light BiVO4 photocatalyst for an enhanced photoelectrochemical water splitting. The Journal of Physical Chemistry Letters, 1(17), pp.2607-2612.

Palacio, L., Pradanos, P., Calvo, J.I. and Hernandez, A., (1999). Porosity measurements by a gas penetration method and other techniques applied to membrane characterization. Thin Solid Films, 348(1-2), pp.22-29.

Paul Glover (2017) Formation Evaluation MSc Course Notes.

Qu, Y., Haibin Y., Nan Y., Yuzun F., Hongyang Z., and Guangtian Z. (2006). "The Effect of Reaction Temperature on the Particle Size, Structure and Magnetic Properties of Coprecipitated $CoFe_2o_4$ Samples." Materials Letters 60, no. (29–30): 3548-52.

Rossetti, R., Nakahara, S., & Brus, L. E. (1983). Quantum size effects in the redox potentials, resonance Raman spectra, and electronic spectra of Cods crystallites in aqueous solution. The Journal of Chemical Physics, 79(2); 1086-1088.

Saion, E., and Elham G. (2011). "On the Theory of Metal Samples Based on Quantum Mechanical Calculation." Malaysian Journal of Fundamental and Applied Sciences 7, no. 1.

Scheinost, A.C., (2005). Metal oxides. In Encyclopedia of Soils in the Environment (pp. 428-438). Elsevier Academic Press netherland.

Shyuada A. (2013). Synthesis and characterization of $MCr_2O_4$ (M= Ni, Co) by thermal treatment method. (Master thesis) Universiti Putra Malaysia.

Smith, R. A. (1978). Semiconductors second edit. Cambridge University Press UK.

Takagaki, A., Tagusagawa, C., Hayashi, S., Hara, M. and Domen, K., (2010). Nanosheets as highly active solid acid catalysts for green chemical syntheses. Energy & Environmental Science, 3(1), pp.82-93.

Tauc, J. (1974). Amorphous and Liquid Semiconductors London: Plenum Press UK.

Velmurugan, R. and Incharoensakdi, A., (2018). Nanoparticles and Organic Matter: Process and Impact. In Nanomaterials in Plants, Algae, and Microorganisms (pp. 407-428). Academic Press.

Whiffen, D.H., (1971). accurate molecular geometry. Chemistry in Britain, 7(2), p.57.

White, A. D. (2006). High-pressure study of spinel chromate (Doctoral dissertation) texas tech university US.

Yadav, T. and Pfaffenbach, K, (2006), NanoProducts Corp. Methods for modifying the surface area of nanomaterials. U.S. Patent 7,007,872.

Yamasaki, Y., Miyasaka, S., Kaneko, Y., He, J.-P., Arima, T., Tokura, Y. (2013). Magnetic reversal of the ferroelectric polarization in a multiferroic spinel oxide. Phys. Rev. Lett. 96, 207204

Yang, X.H., Yang, H.G. and Lou, X.W., (2009). Top-down fabrication of $\alpha$-$Fe_2O_3$ single-crystal nanodiscs and microparticles with tunable porosity for largely improved lithium storage properties. Journal of the American Chemical Society, 132(38), pp.13162-13164.